Research Paper
Computational Methods for Differential Equations
http://cmde.tabrizu.ac.ir
Vol. 12, No. 4, 2024, pp. 669-686
DOI:10.22034/cmde.2024.57085.2388

A numerical investigation for the COVID-19 spatiotemporal lockdown-vaccination model

Ahmed F. Koura[1], Kamal R. Raslan[2], Khalid K. Ali[2,*] and Mohamed Abozeid Shaalan[3]

[1]Basic Science Department, Al-Safwa High Institute of Engineering, Egypt.

[2]Mathematics Department, Faculty of Science, Al-Azhar University, Nasr-City, Cairo, Egypt.

[3]Higher Technological Institute, Tenth of Ramadan City, Egypt.

Abstract

The present article investigates a numerical analysis of COVID-19 (temporal and spatio-tempora) lockdown-vaccination models. The proposed models consist of six nonlinear ordinary differential equations as a temporal model and six nonlinear partial differential equations as a spatio-temporal model. The evaluation of reproduction number is a forecast spread of the COVID-19 pandemic. Sensitivity analysis is used to emphasize the importance of pandemic parameters. We show the stability regions of the disease-free equilibrium point and pandemic equilibrium point. We use effective methods such as central finite difference (CFD) and Runge-Kutta of fifth order (RK-5). We apply Von-Neumann stability and consistency of the numerical scheme for the spatio-temporal model. We examine and compare the numerical results of the proposed models under various parameters.

Keywords. COVID-19 mathematical model, Reproduction number, Sensitivity analysis, Central finite method, Runge Kutta of fifth order method, Von-Neumann stability.

2010 Mathematics Subject Classification. 34Bxx, 65Lxx, 65Mxx.

1. Introduction

All over the world, there are a great number of viruses, including COVID-19, which has infected millions of people and affected their health and the economy as well. Many natural phenomena and life problems are crystallized in the form of mathematical models that are dealt with analytically or numerically [1, 3–5, 7, 8, 13]. The transmission dynamics of the virus can be formulated in mathematical models that understand us and predict the dynamics of the virus [10–12, 14, 19]. In [15] Kucharski et al. combined datasets from inside and outside Wuhan and formulated it as a mathematical model to estimate the early dynamics of transmission of the infection and take control measures against the spread of the virus. Baba et al. applied some schemes such as ODE45, Euler, RK-2, and RK-4 to a mathematical model of COVID-19 that represents the imposition of lockdown in Nigeria [6]. In Brazil, Valle [22] used an iterative method in the COVID-19 model that can estimate the total number of infections and deaths, and the observed data are in agreement with the results obtained by the Gompertz model. Mandal et al. [17] found that to control COVID-19 in India by reducing the contact of exposed and susceptible humans to avoid imposing control measures by the government, In [9] Biswas et al. studied a model of the spreading of COVID-19, they estimated the parameters of the model by fitting the model with collected data about the virus in India and presented predictions with the future trends of COVID-19 transmission under some control measures. Zhang et al.[24] applied Runge-Kutta of fourth-order to evaluate and analyze a new fractional-order mathematical model for the COVID-19 pandemic. Agarwal et al. analyzed the COVID-19 mathematical model of fractional order theoretically [2]. In [23] Wrapp et al. showed that the infected people who show symptoms are more numerous than those who do not show symptoms. Rothe et al. [20] discovered that the COVID-19 virus has more links than the SARS virus. In [18] Hakimeh et al. introduced a mathematical model to reduce the transmission of some diseases by the Caputo fractional-order

Received: 12 June 2023 ; Accepted: 27 March 2024.
∗ Corresponding author. Email: khalidkaram2012@yahoo.com .

derivative. A numerical simulation was presented by Tuan et al. in [21] which obtained the approximate solutions by using the generalized Adams-Bashforth-Moulton method.In [16] Banan et al. introduced the multistep Laplace optimized decomposition method, applied to a COVID-19 model with fractional derivatives, the method is found to be highly accurate compared to the traditional fourth-order Runge-Kutta method.

This article is arranged as follows: In section 2, we present a mathematical formulation for the COVID-19 lockdown-vaccination (temporal and spatiotemporal) models. We investigate reproduction number, sensitivity analysis, and stability region analysis for the presented model, as shown in section 3. In section 4, we introduce numerical solutions for the COVID-19 temporal model via two schemes: Runge-Kutta of fifth order and the central finite difference. In section 5, we introduce numerical solutions for the COVID-19 spatiotemporal model, study the stability, and consistency of the numerical scheme, and discuss the results of the proposed model. In section 6, we discuss the effect of some parameters on controlling the spread of infection between individuals.

2. Mathematical formulation

In this section, we introduce a mathematical model of COVID-19 that describes the effect of lockdown and vaccination strategies on the spread of COVID-19 between people. The population is divided into six categories: $S(t)$ represents the susceptible people who are not under lockdown, $S_Q(t)$ represents susceptible persons who are already under lockdown, $I(t)$ represents infected people who are not under lockdown, $I_Q(t)$ represents infected persons who are under lockdown at the same time, $Q(t)$ is the cumulative density of the lockdown program, and $V(t)$ represents vaccinated people. This model can be covered by a system of six nonlinear ordinary differential equations as a temporal model and a system of six nonlinear partial differential equations as a spatiotemporal model.

2.1. **Temporal model.**

$$\begin{aligned}
\frac{dS}{dt} &= \Lambda + \beta_v V - \beta SI - \delta_s SQ - (d+\beta_s)S + \mu_i I + \mu_q I_Q + \nu_s S_Q,\\
\frac{dS_Q}{dt} &= \delta_s SQ - dS_Q - \nu_s S_Q - \beta_{S_Q} S_Q,\\
\frac{dI}{dt} &= \beta SI - \mu_i I - \rho_i I - dI - \delta_i IQ + \nu_i I_Q,\\
\frac{dI_Q}{dt} &= \delta_i IQ - dI_Q - \nu_i I_Q - \mu_q I_Q - \rho_q I_Q,\\
\frac{dQ}{dt} &= \eta I - \psi Q,\\
\frac{dV}{dt} &= \beta_s S + \beta_{S_Q} S_Q - dV - \beta_v V.
\end{aligned} \tag{2.1}$$

Subject to non-negative initial conditions:

$$S(0) = S_0, S_Q(0) = S_{Q_0}, I(0) = I_0, I_Q(0) = I_{Q_0}, Q(0) = Q_0, V(0) = V_0. \tag{2.2}$$

2.2. **Spatiotemporal model.**

$$\begin{aligned}
\frac{\partial S}{\partial t} &= C_1\frac{\partial^2 S}{\partial x^2} + \Lambda + \beta_v V - \beta SI - \delta_s SQ - (d+\beta_s)S + \mu_i I + \mu_q I_Q + \nu_s S_Q,\\
\frac{\partial S_Q}{\partial t} &= C_2\frac{\partial^2 S_Q}{\partial x^2} + \delta_s SQ - dS_Q - \nu_s S_Q - \beta_{S_Q} S_Q,\\
\frac{\partial I}{\partial t} &= C_3\frac{\partial^2 I}{\partial x^2} + \beta SI - \mu_i I - \rho_i I - dI - \delta_i IQ + \nu_i I_Q,\\
\frac{\partial I_Q}{\partial t} &= C_4\frac{\partial^2 I_Q}{\partial x^2} + \delta_i IQ - dI_Q - \nu_i I_Q - \mu_q I_Q - \rho_q I_Q,\\
\frac{\partial V}{\partial t} &= C_6\frac{\partial^2 V}{\partial x^2} + \beta_s S + \beta_{S_Q} S_Q - dV - \beta_v V.
\end{aligned} \tag{2.3}$$

With initial conditions,

$$\begin{aligned}
S(0,x) &= \begin{cases} 2S_0x & 0 \le x \le 0.5, \\ 2S_0(1-x) & 0.5 \le x \le 1, \end{cases} \\
S_Q(0,x) &= \begin{cases} 2S_{Q_0}x & 0 \le x \le 0.5, \\ 2S_{Q_0}(1-x) & 0.5 \le x \le 1, \end{cases} \\
I(0,x) &= \begin{cases} 2I_0x & 0 \le x \le 0.5, \\ 2I_0(1-x) & 0.5 \le x \le 1, \end{cases} \\
I_Q(0,x) &= \begin{cases} 2I_{Q_0}x & 0 \le x \le 0.5, \\ 2I_{Q_0}(1-x) & 0.5 \le x \le 1, \end{cases} \\
Q(0,x) &= \begin{cases} 2Q_0x & 0 \le x \le 0.5, \\ 2Q_0(1-x) & 0.5 \le x \le 1, \end{cases} \\
V(0,x) &= \begin{cases} 2V_0x & 0 \le x \le 0.5, \\ 2V_0(1-x) & 0.5 \le x \le 1. \end{cases}
\end{aligned} \tag{2.4}$$

And homogeneous Neumann boundary conditions,

$$\begin{aligned}
&\frac{\partial S(t,0)}{\partial x} = \frac{\partial S(t,1)}{\partial x} = 0, \\
&\frac{\partial S_Q(t,0)}{\partial x} = \frac{\partial S_Q(t,1)}{\partial x} = 0, \\
&\frac{\partial I(t,0)}{\partial x} = \frac{\partial I(t,1)}{\partial x} = 0, \\
&\frac{\partial I_Q(t,0)}{\partial x} = \frac{\partial I_Q(t,1)}{\partial x} = 0, \\
&\frac{\partial Q(t,0)}{\partial x} = \frac{\partial Q(t,1)}{\partial x} = 0, \\
&\frac{\partial V(t,0)}{\partial x} = \frac{\partial V(t,1)}{\partial x} = 0.
\end{aligned} \tag{2.5}$$

Where the parameters definitions as shown in Table 1.

3. Reproduction number and stability region

In this section, we introduce some important indicators that help us realize the spread of the pandemic in the population.

3.1. **Reproduction number.** The number of new infections caused by an infectious individual in a disease-free population is defined as the reproduction number R_0. The reproduction number in pandemic mathematical models represents the average number of secondary infections produced by a single infected individual in a completely susceptible population. If $R_0 > 1$, the pandemic will spread, while it will be confined if $R_0 < 1$. Adjusting interventions to lower R_0 helps control and mitigate the impact of a pandemic, making it a crucial parameter in mathematical modeling for public health planning and response strategies.
To obtain R_0 for the proposed model (2.1) we put the virus-free equilibrium point $C_0 = [S_0, 0, 0, 0, V_0]$ and make the

TABLE 1. Parameters definitions.

Symbol	Definition
Λ	Rate of recruitment
β	Rate of infection contact
δ_s	Lockdown imposition on susceptible people
δ_i	Lockdown imposition on infected people
ρ_i	Rate of death in infected persons but not under lockdown
ρ_q	Rate of death in infected persons under lockdown
ρ_q	Rate of death in infected persons under lockdown
μ_i	Rate of recovery in infected persons but not under lockdown
μ_q	Rate of recovery in infected persons under lockdown
ν_s	Transfer rate of susceptible lockdown persons to susceptible class
ν_i	The rate of infection of persons under lockdown to the infection class
η	Transfer rate of infection of persons under lockdown to infection class
η	Achievement rate of the lockdown program
ψ	Depletion rate of the lockdown program
β_s	Vaccination rate in S class
β_{S_Q}	Vaccination rate in S_Q class
β_v	Vaccine waning rate
d	Natural death rate

system (2.1) equal to zero and solve it.

$$\begin{aligned}
0 &= \Lambda + \beta_v V - \beta SI - \delta_s SQ - (d+\beta_s)S + \mu_i I + \mu_q I_Q + \nu_s S_Q,\\
0 &= \delta_s SQ - dS_Q - \nu_s S_Q - \beta_{S_Q} S_Q,\\
0 &= \beta SI - \mu_i I - \rho_i I - dI - \delta_i IQ + \nu_i I_Q,\\
0 &= \delta_i IQ - dI_Q - \nu_i I_Q - \mu_q I_Q - \rho_q I_Q,\\
0 &= \eta I - \psi Q,\\
0 &= \beta_s S + \beta_{S_Q} S_Q - dV - \beta_v V.
\end{aligned} \tag{3.1}$$

we get $S_0 = \frac{\Lambda}{d+\beta_s}$ and $V_0 = \frac{\beta_s S_0}{d+\beta_v}$.
Let $\mathrm{X} = [I, I_Q]^T$ which I and I_Q are components of the infection in the model and

$$\frac{d\mathrm{X}}{dt} = \mathrm{F}(\mathrm{X}) - \mathrm{V}(\mathrm{X}), \tag{3.2}$$

where $\mathrm{F}(\mathrm{X}) = \begin{pmatrix} \beta SI - \delta_i IQ \\ \delta_i IQ \end{pmatrix}$, $\mathrm{V}(\mathrm{X}) = \begin{pmatrix} \mu_i I + \rho_i I + dI - \nu_i I_Q \\ dI_Q + \nu_i I_Q + \mu_q I_Q + \rho_q I_Q \end{pmatrix}$.

$$J(\mathrm{F}(\mathrm{X})) = \begin{pmatrix} \beta S - \delta_i Q & 0 \\ \delta_i Q & 0 \end{pmatrix}, J(\mathrm{V}(\mathrm{X})) = \begin{pmatrix} \mu_i + \rho_i + d & -\nu_i \\ 0 & d + \nu_i + \mu_q + \rho_q \end{pmatrix}, \tag{3.3}$$

where $J(\mathrm{F}(\mathrm{X}))$ and $J(\mathrm{V}(\mathrm{X}))$ are the Jacobians of $\mathrm{F}(\mathrm{X})$ and $\mathrm{V}(\mathrm{X})$ respectively.
We calculate the greatest eigenvalue of the matrix $J(\mathrm{F}(\mathrm{X})) * J(\mathrm{V}(\mathrm{X}))^{-1}$ and substitute with C_0, we obtain the reproduction number R_0 for the model (2.1).

$$R_0 = \frac{\beta\Lambda}{(d+\beta_s)\rho_i + d(d+\beta_s) + (d+\beta_s)\mu_i}. \tag{3.4}$$

3.2. **Sensitivity analysis.** The sensitivity analysis is studying the pandemic parameters of the proposed model (2.1) and their effects on the virus spread. Using the reproduction number R_0 we obtain

$$\begin{aligned}
\frac{\partial R_0}{\partial \Lambda} &= \frac{\beta}{(d+\beta_s)(d+\mu_i+\rho_i)},\\
\frac{\partial R_0}{\partial \beta} &= \frac{\Lambda}{(d+\beta_s)(d+\mu_i+\rho_i)},\\
\frac{\partial R_0}{\partial d} &= -\frac{\beta\Lambda(2d+\mu_i+\rho_i+\beta_s)}{(d+\beta_s)^2(d+\mu_i+\rho_i)^2},\\
\frac{\partial R_0}{\partial \rho_i} &= -\frac{\beta\Lambda}{(d+\beta_s)(d+\mu_i+\rho_i)^2},\\
\frac{\partial R_0}{\partial \mu_i} &= -\frac{\beta\Lambda}{(d+\beta_s)(d+\mu_i+\rho_i)^2},\\
\frac{\partial R_0}{\partial \beta_s} &= -\frac{\beta\Lambda}{(d+\beta_s)^2(d+\mu_i+\rho_i)}.
\end{aligned} \tag{3.5}$$

Given that all parameters are positive, then we have $\frac{\partial R_0}{\partial \Lambda} > 0$, $\frac{\partial R_0}{\partial \beta} > 0$ and $\frac{\partial R_0}{\partial d} < 0$, $\frac{\partial R_0}{\partial \rho_i} < 0$, $\frac{\partial R_0}{\partial \mu_i} < 0$, $\frac{\partial R_0}{\partial \beta_s} < 0$. Thus, increasing the parameters Λ and β results in an increase in R_0, and increasing the parameters d, ρ_i, β_s, and μ_i leads to a decrease in R_0.

3.3. **Stability region.** In the stability regions of the disease-free equilibrium point and pandemic equilibrium point as shown in Figures 1 and 2 for (ρ_i,μ_i,β) and the values of other parameters are fixed. In Figure 1(a), we examine the effects of (ρ_i,μ_i,β) at the disease-free equilibrium point where $R_0 < 1$. Figures 1(b), 1(c), and 1(d) illustrates the projection of the stability region (ρ_i,β) with fixed μ_i at 0.15, 0.25, and 0.45, respectively. We observe that ρ_i and β maintain their stability at a large value of μ_i.
In Figure 2(a), we examine the effects of (ρ_i,μ_i,β) at the endemic equilibrium point. Figures 2(b), 2(c), and 2(d) illustrates the projection of the stability region (ρ_i,β) with fixed μ_i at 0.15, 0.25, and 0.45, respectively. We observe that ρ_i and β maintain their stability at a small value of μ_i.

4. Numerical solutions for temporal model

This section presents the computational methods of the temporal model (2.1). We take some parameter values from the works of literature and estimate the other parameter values from the stability region, which is discussed in section 3. We carry out two efficient numerical schemes: Runge-Kutta fifth-order and central finite-difference.
The main characteristics of the fifth-order Runge-Kutta method provide a higher degree of stability, making it effective in handling ODEs. ODEs often require smaller step sizes to maintain accuracy, but the 5th-order Runge-Kutta method can still provide accurate results even with relatively larger step sizes compared to lower-order methods. The main characteristics of the central finite difference methods are accuracy and stability. Higher-order methods approximate derivatives using more points, leading to smaller errors. They are also often more numerically stable, allowing a larger timestep size. This improves computational efficiency by enabling the use of a coarser grid for a given accuracy.

4.1. **Runge-Kutta Of fifth-order (RK-5) method.** Assume that the initial value problem is well-posed, then

$$\frac{dy}{dt} = F(t,y), a < t < b, y(a) = e, \tag{4.1}$$

Algorithm Steps:
Step 1:
Discretize the Domain by dividing the domain of $t \in [0, 200]$ with step size $\tau = 1$.

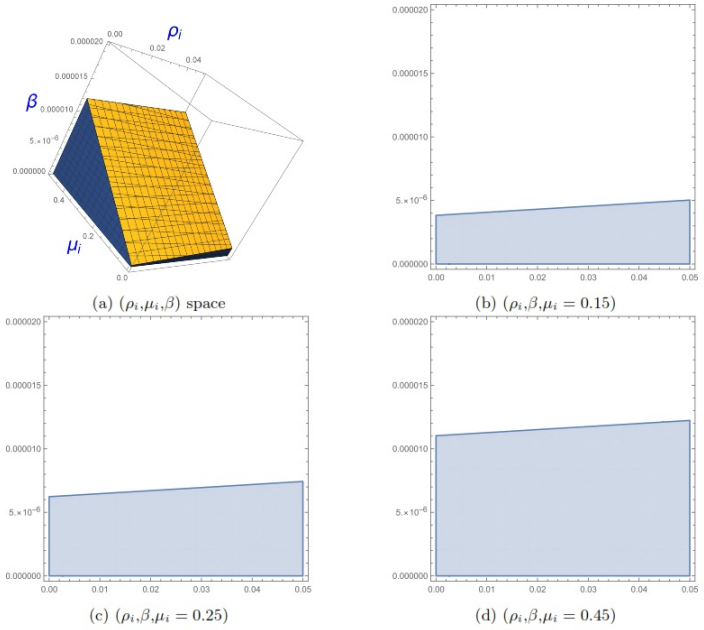

FIGURE 1. Stability region for disease free equilibrium point.

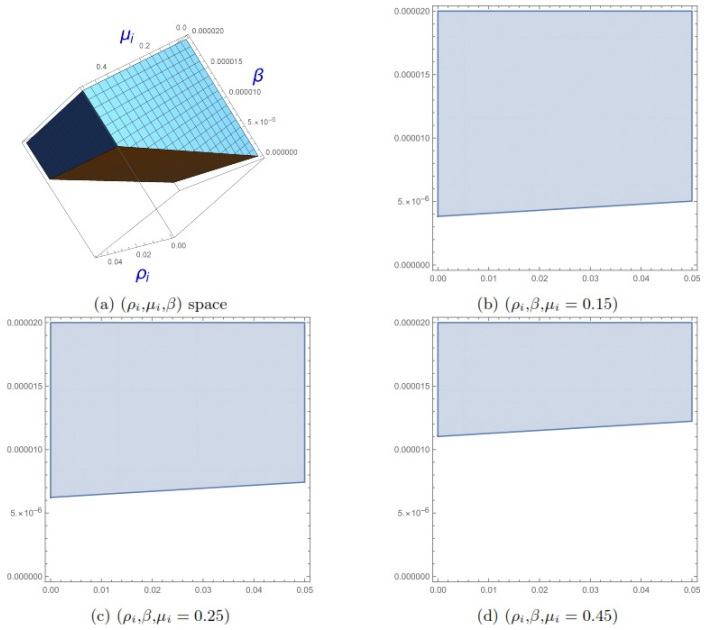

FIGURE 2. Stability region for pandemic equilibrium point.

Step 2:
We establish the RK-5 technique, for each time step compute a sequence of approximation points

$$\begin{aligned}
k_1 &= F(t_i, w_i),\\
k_2 &= F(t_i + \frac{h}{4}, w_i + \frac{k_1 h}{4}),\\
k_3 &= F(t_i + \frac{h}{4}, w_i + \frac{k_1 h}{8} + \frac{k_2 h}{8}),\\
k_4 &= F(t_i + \frac{h}{2}, w_i - \frac{k_2 h}{2} + k_3 h),\\
k_5 &= F(t_i + \frac{3h}{4}, w_i + \frac{3k_1 h}{16} + \frac{9k_4 h}{16}),\\
k_6 &= F(t_i + h, w_i - \frac{3k_1 h}{7} + \frac{2k_2 h}{7} + \frac{12k_3 h}{7} - \frac{12k_4 h}{7} + \frac{8k_5 h}{7}).
\end{aligned} \tag{4.2}$$

Step 3:
Update the variables using the weighted sum of the K values,

$$w_{i+1} = w_i + \frac{h}{90}(7k_1 + 32k_3 + 12k_4 + 32k_5 + 7k_6). \tag{4.3}$$

Step 4:
Update time

$$t_{i+1} = t_i + \tau. \tag{4.4}$$

Step 5:
Repeat steps 2-4 until you reach the desired endpoint or number of time steps.
We use Mathematica 12 to maintain numerical results for RK-5 as shown in Figure 3.

4.2. **Central finite difference (CFD) method.** Suppose that a well-posed IVP (4.1) is given the CFD technique as a sequence of approximation points $(t, w_i) \simeq (t, y(t))$ to the exact solution of Equation (4.1) by

$$\begin{aligned}
t_{i+1} &= t_i + k,\\
\frac{dy}{dt} &= \frac{F(t_i, w_i + k) + F(t_i, w_i - k)}{2k}.
\end{aligned}$$

Step 1:
Discretize the Domain by dividing the domain of $t \in [0, 200]$ with step size $\tau = 1$.
Step 2:
Apply the central finite difference method to approximate the derivatives in the differential equations. For each equation in the system, replace the derivatives with central finite difference approximations.
Step 3:
Discretize the system of equations and Convert it into a system of algebraic equations.

$$(S)_{n+1} = (S)_{n-1} + 2\tau\left(\Lambda - \beta(S)_n(I)_n - \delta_s(S)_n(Q)_n - d(S)_n + \mu_i(I)_n + \mu_q(I_Q)_n + \nu_s(S_Q)_n\right), \tag{4.5}$$

$$(S_Q)_{n+1} = (S_Q)_{n-1} + 2\tau\left(\delta_s(S)_n(Q)_n - d(S_Q)_n - \nu_s(S_Q)_n\right), \tag{4.6}$$

$$I_{n+1} = I_{n-1} + 2\tau\left(\beta(S)_n I_n - \mu_i I_n - \rho_i I_n - dI_n - \delta_i I(Q)_n + \nu_i(I_Q)_n\right), \tag{4.7}$$

$$(I_Q)_{n+1} = (I_Q)_{n-1} + 2\tau\left(\delta_i I_n Q_n - d(I_Q)_n - \nu_i(I_Q)_n - \mu_q(I_Q)_n - \rho_q(I_Q)_n\right), \tag{4.8}$$

$$Q_{n+1} = Q_{n-1} + 2\tau\left(\eta I_n - \psi Q_n\right). \tag{4.9}$$

$$V_{n+1} = V_{n-1} + 2\tau\left(\beta_s(S)_n + \beta_{S_Q}(S_Q)_n - dV_n - \beta_v V_n\right). \tag{4.10}$$

Step 4:
Solve the algebraic system.
Step 5:
Update the values of the variables at each grid point based on the solution obtained.
Step 6:
Repeat iteratively.
We use Mathematica 12 to maintain numerical results for system (2.1) using the CFD method as shown in Figure 4.

4.3. **Results.** Now, we discuss the numerical outcomes of the governing model with respect to the approximate solutions. To achieve this aim, we employed the effective Central Finite Difference and RK-5 schemes and compared the results after 200 days. The initial conditions as discussed in [6] are $S(0) = 400, S_Q(0) = 300, I(0) = 300, I_Q(0) = 497$, $Q(0) = 200$, and $V(0) = 120$, and the parameter values are $\Lambda = 400, \delta_s = 0.0002, \nu_s = 0.2, \eta = 0.0005, \psi = 0.06$, $\mu_i = \mu_q = 0.16979, \rho_q = 0.03275$, $\delta_i = 0.002, \nu_i = 0.02$, $d = 0.0096$, and assuming the values of $\beta = 0.000017$, $\rho_i = 0.03275$. Using the Mathematica package, we apply our techniques of CFD and RK-5 to solve the proposed model (2.1).
Figures 3 and 4 represent the solution of the system (2.1) with RK5 and CFD methods respectively. Figure 5 represents compare between RK5 and CFD results of the solution of the system (2.1). It can be demonstrated that the RK-5 method gives a better approximation than the CFD method.

All figures show that the results of the model converge to their equilibrium points.
In Figure 6, we introduce solutions with different values of $\delta_i = 0.002, 0.001$, and 0.003 that represent the imposition of lockdown on infected individuals to support the validity of our results.

Finally, from all the figures, we can confirm the effectiveness of the proposed algorithms and their computationally appropriate use of numerical handling of the given model.

5. Numerical solutions for spatiotemporal model

In this section, we present a numerical simulation of the spatiotemporal model (2.3) with initial conditions (2.4) and boundary conditions (2.5).
Step1:
Beginning with dividing the domain of $x \in [0, 1]$ and $t \in [0, 200]$ into $10^2 \times 200$ cubes with step size $h = 0.1$ and $\tau = 1$. For this, we apply finite difference using

$$\begin{aligned}
\frac{\partial f(t,x)}{\partial t} &= \frac{f_i^{n+1} - f_i^n}{\tau}, \\
\frac{\partial^2 f(t,x)}{\partial x^2} &= \frac{f_{i-1}^{n+1} - 2f_i^{n+1} + f_{i+1}^{n+1}}{h^2}, \\
\frac{\partial f(t,x)}{\partial x} &= \frac{f_{i+1}^n - f_{i-1}^n}{2h}.
\end{aligned} \tag{5.1}$$

Step 2: Discretizing the system and its boundary conditions we get the following results,

$$\begin{aligned}
(S)_i^{n+1} &= (S)_i^n + \frac{\tau C_1}{h^2}((S)_{i+1}^{n+1} - 2(S)_i^{n+1} + (S)_{i-1}^{n+1}) + \tau(\Lambda - \beta(S)_i^{n+1}(I)_i^n \\
&- \delta_s(S)_i^{n+1}(Q)_i^n - (d + \beta_s)(S)_i^{n+1} + \mu_i(I)_i^n + \mu_q(I_Q)_i^n + \nu_s(S_Q)_i^{n+1} + \beta_v(V)_i^n),
\end{aligned} \tag{5.2}$$

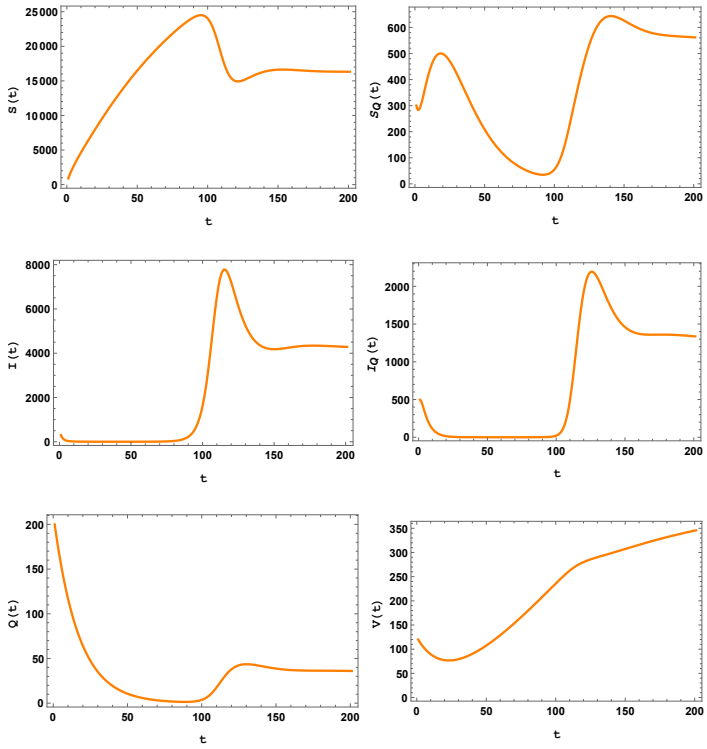

FIGURE 3. Numerical results for system (2.1) using RK-5 method.

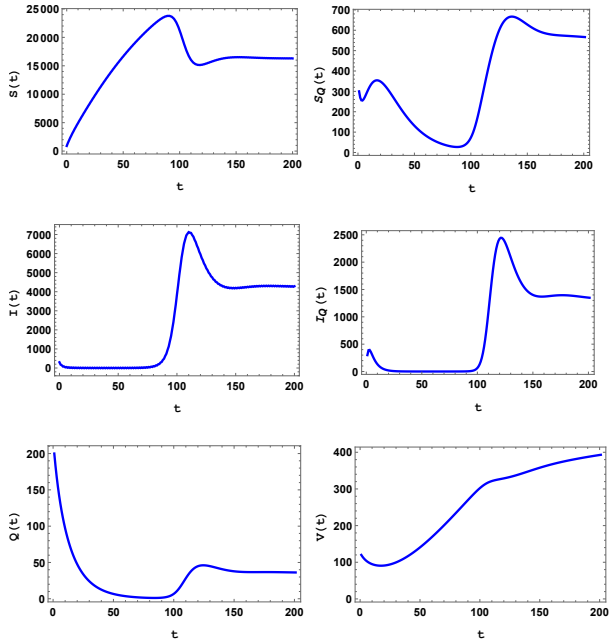

FIGURE 4. Numerical results for system (2.1) using CFD method.

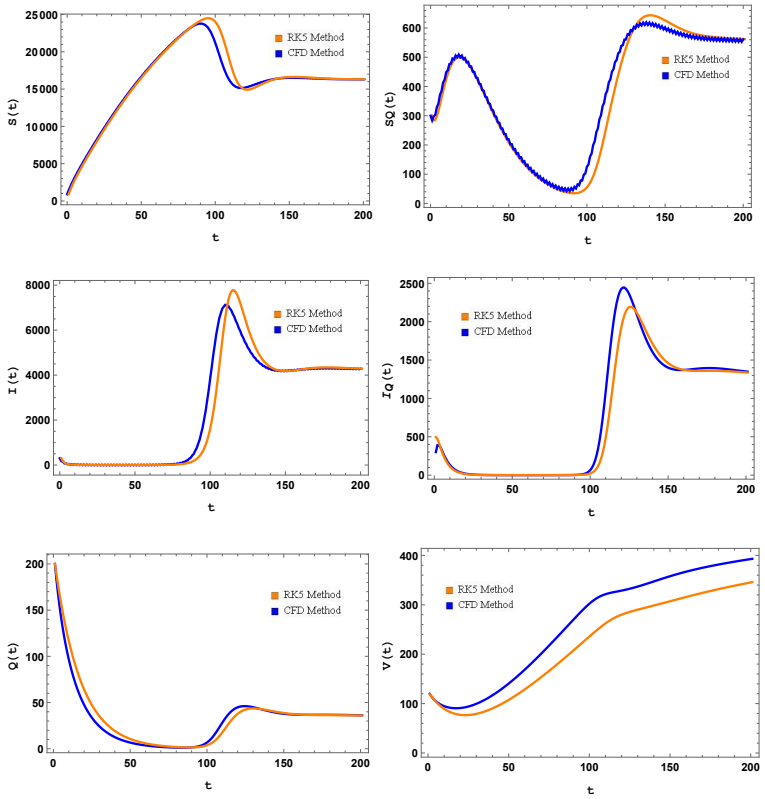

FIGURE 5. RK-5 method versus CFD method for model (2.1).

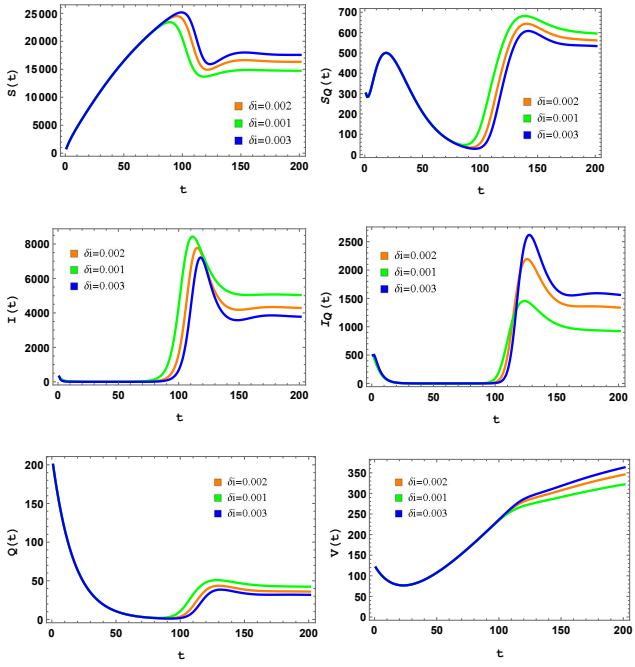

FIGURE 6. Compare between different values of δ_i for model (2.1).

$$\begin{aligned}(S_Q)_i^{n+1} &= (S_Q)_i^n + \frac{\tau C_2}{h^2}((S_Q)_{i+1}^{n+1} - 2(S_Q)_i^{n+1} + (S_Q)_{i-1}^{n+1}) + \tau(I_i^{n+1}\delta_s(S)_i^n(Q)_i^n \\ &- d(S_Q)_i^{n+1} - \nu_s(S_Q)_i^{n+1} - \beta_{S_Q}(S_Q)_i^{n+1}),\end{aligned} \tag{5.3}$$

$$\begin{aligned}I_i^{n+1} &= I_i{}^n + \frac{\tau C_3}{h^2}(I_{i+1}^{n+1} - 2I_i^{n+1} + I_{i-1}^{n+1}) + \tau(\beta(S)_i^n I_i^{n+1} - \mu_i I_i^{n+1} - \rho_i I_i^{n+1} \\ &- dI_i^{n+1} - \delta_i I(Q)_i^n + \nu_i(I_Q)_i^n),\end{aligned} \tag{5.4}$$

$$\begin{aligned}(I_Q)_i^{n+1} &= (I_Q)_i^n + \frac{\tau C_4}{h^2}((I_Q)_{i+1}^{n+1} - 2(I_Q)_i^{n+1} + (I_Q)_{i-1}^{n+1}) + \tau(\delta_i I_i{}^n Q_i{}^n \\ &- d(I_Q)_i^{n+1} - \nu_i(I_Q)_i^{n+1} - \mu_q(I_Q)_i^{n+1} - \rho_q(I_Q)_i^{n+1}),\end{aligned} \tag{5.5}$$

$$Q_i^{n+1} = Q_i{}^n + \frac{\tau C_5}{h^2}(Q_{i+1}^{n+1} - 2Q_i^{n+1} + Q_{i-1}^{n+1}) + \tau(\eta I_i{}^n - \psi Q_i^{n+1}), \tag{5.6}$$

$$\begin{aligned}V_i^{n+1} &= V_i{}^n + \frac{\tau C_6}{h^2}(V_{i+1}^{n+1} - 2V_i^{n+1} + V_{i-1}^{n+1}) + \tau(\beta_s(S)_i^n + \beta_{S_Q}(S_Q)_i^n \\ &- \beta_v V_i^{n+1} - dV_i^{n+1}).\end{aligned} \tag{5.7}$$

Step 4:
Solve the algebraic system.
Step 5:
Update the values of the variables at each grid point based on the solution obtained.
Step 6:
Repeat iteratively.

5.1. **Stability of numerical scheme.** In this subsection, we will test Von Neumann stability for the numerical method that we have applied.
Von-Neumann stability refers to a criterion used in numerical analysis to ensure the stability of finite difference methods when solving partial differential equations. Named after mathematician John von Neumann, it involves analyzing the amplification factor of numerical errors over iterations. Meeting the stability criteria helps prevent uncontrolled growth of errors and ensures reliable and accurate numerical simulations.
Assume

$$\begin{aligned}S_i^n &= \xi_1^n e^{Jk_s ih}, \\ S_i^{n+1} &= \xi_1^{n+1} e^{Jk_s ih}, \\ S_{i+1}^n &= \xi_1^n e^{Jk_s (i+1)h}, \\ S_{i-1}^n &= \xi_1^n e^{Jk_s (i-1)h},\end{aligned} \tag{5.8}$$

substitute from (5.8) in Equation (5.2) we get the following relation,

$$\begin{aligned}\xi_1^{n+1} e^{Jk_s ih} &= \xi_1^n e^{Jk_s ih} + \frac{\tau C_1}{h^2}(\xi_1^{n+1} e^{Jk_s (i+1)h} - 2\xi_1^{n+1} e^{Jk_s ih} + \xi_1^{n+1} e^{Jk_s (i-1)h}) + \Lambda \\ &- \beta\xi_1^{n+1} e^{Jk_s ih}(I)_i^n - \delta_s \xi_1^{n+1} e^{Jk_s ih}(Q)_i^n - (\beta_s + d)\xi_1^{n+1} e^{Jk_s ih} + \mu_i(I)_i^n + \mu_q(I_Q)_i^n \\ &+ \nu_s(S_Q)_i^n + \beta_v(V)_i^n.\end{aligned} \tag{5.9}$$

Define the amplification factor $G_1 = \frac{S_i^{n+1}}{S_i^n}$, we can compute G_1 by dividing Equation (5.9) by S_i^n and obtain

$$\begin{aligned}G_1 &= 1 + \frac{\tau C_1}{h^2}(G_1 e^{Jk_S h} - 2G_1 + G_1 e^{-Jk_S h}) + \Lambda - \beta G_1(I)_i^n - \delta_s G_1(Q)_i^n - (\beta_s + d)G_1 \\ &+ \mu_i(I)_i^n + \mu_q(I_Q)_i^n + \nu_s(S_Q)_i^n + \beta_v(V)_i^n,\end{aligned} \tag{5.10}$$

$$G_1 = \frac{1}{1 + 4\frac{\tau C_1}{h^2} sin^2(\frac{k_{S_a} h}{2}) + \tau(\upsilon_a^{\cdot} + d + \beta_s)}, \tag{5.11}$$

$$G_1 = \left| \frac{1}{1 + 4\frac{\tau C_1}{h^2} sin^2(\frac{k_{S_a} h}{2}) + \tau(\upsilon_a^{\cdot} + d + \beta_s)} \right| \leq 1. \tag{5.12}$$

Similarly, repeating the previous steps to Equations (5.3), (5.4), (5.5), (5.6), and (5.7) for $(S_Q)_i^n$, I_i^n, $(I_Q)_i^n$ and Q_i^n with $(S_Q)_i^n = \xi_2^n e^{Jk_{s_q} ih}$, $I_i^n = \xi_3^n e^{Jk_I ih}$, $(I_Q)_i^n = \xi_4^n e^{Jk_{(I_Q)} ih}$, $Q_i^n = \xi_5^n e^{Jk_Q ih}$ and $V_i^n = \xi_6^n e^{Jk_V ih}$ respectively, we also obtain

$$G_2 = \left| \frac{1}{1 + 4\frac{\tau C_2}{h^2} sin^2(\frac{k_{S_b} h}{2}) + \tau(d + \beta_{S_Q} + \nu_s)} \right| \leq 1, \tag{5.13}$$

$$G_3 = \left| \frac{1}{1 + 4\frac{\tau C_3}{h^2} sin^2(\frac{k_I h}{2}) + \tau(\mu_i + \rho_i + d + \upsilon_b^{\cdot})} \right| \leq 1, \tag{5.14}$$

$$G_4 = \left| \frac{1}{1 + 4\frac{\tau C_4}{h^2} sin^2(\frac{k_T h}{2}) + \tau(d + \nu_i + \mu_q + \rho_q)} \right| \leq 1, \tag{5.15}$$

$$G_5 = \left| \frac{1}{1 + 4\frac{\tau C_5}{h^2} sin^2(\frac{k_R h}{2}) + \tau\psi} \right| \leq 1, \tag{5.16}$$

$$G_6 = \left| \frac{1}{1 + 4\frac{\tau C_6}{h^2} sin^2(\frac{k_V h}{2}) + d + \beta_v} \right| \leq 1, \tag{5.17}$$

where $\upsilon_a^{\cdot} = \beta {I_i}^n + \delta_s {Q_i}^n$, $\upsilon_b^{\cdot} = \delta_i {Q_i}^n - \beta {S_i}^n$ and $J = \sqrt{-1}$.
So $G_i \leq 1$, $i = 1, 2, 3, 4, 5, 6$ which is the necessary and sufficient condition for the error to remain bounded and maintain von Nemann stability for the numerical method.

5.2. **Consistency.** In this subsection, we will use Taylor expansion to prove that this numerical scheme is first-order consistent in t and second-order consistent in x. For this, we use

$$\begin{aligned} \Phi_S &= \frac{S_i^{n+1} - S_i^n}{\tau} - \frac{C_1}{h^2}(S_{i+1}^{n+1} - 2S_i^{n+1} + S_{j-1}^{n+1}) - \Lambda + \beta(S)_i^{n+1}(I)_i^n \\ &+ \delta_s(S)_i^{n+1}(Q)_i^n + d(S)_i^{n+1} - \mu_i(I)_i^n - \mu_q(I_Q)_i^n - \nu_s(S_Q)_i^{n+1}, \end{aligned} \tag{5.18}$$

$$\begin{aligned} \Phi_S &= (\frac{\partial S}{\partial t} + \frac{\tau}{2!}\frac{\partial^2 S}{\partial t^2} + \frac{\tau^2}{3!}\frac{\partial^2 S}{\partial t^2} + ...) - \frac{C_1}{h^2}(h^2(\frac{\partial^2 S}{\partial x^2} + 2\frac{h^2}{4!}\frac{\partial^4 S}{\partial x^2} + ...)) \\ &- \Lambda + \beta(I)_i^n + \delta_s(Q)_i^n + d - \nu_s * ({S_i}^n + \tau\frac{\partial S}{\partial t} + \frac{\tau^2}{2!}\frac{\partial^2 S}{\partial t^2} + \frac{\tau^3}{3!}\frac{\partial^2 S}{\partial t^2} + ...), \end{aligned} \tag{5.19}$$

$$\Phi_S = -\frac{C_1 h^2}{12}(\frac{\partial^4 S}{\partial x^4}) + \tau((\beta I_i^n + \delta_s Q_i^n + d)\frac{\partial S_a}{\partial t} + ...), \tag{5.20}$$

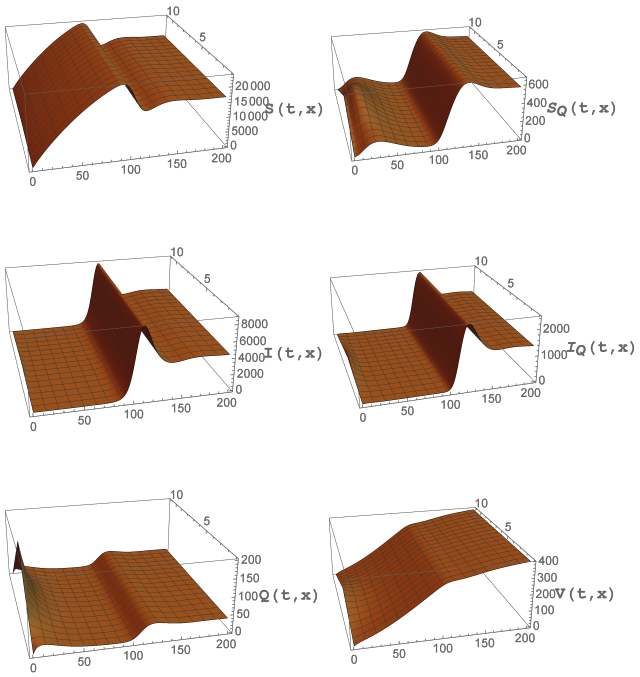

FIGURE 7. Numerical simulation results for disease free equilibrium point for model (2.3).

which devolve to zero as τ,h becomes zero.
Also, we can obtain the relations of S_Q, I, I_Q, and Q using the previous steps as follows:

$$\begin{aligned}
\Phi_{S_Q} &= -\frac{C_2h^2}{12}\left(\frac{\partial^4 S_Q}{\partial x^4}\right) + \tau(\alpha_b I_i^n + \delta)\left(\frac{\partial S_Q}{\partial t} + ...\right),\\
\Phi_I &= -\frac{C_3h^2}{12}\left(\frac{\partial^4 I}{\partial x^4}\right) + \tau(\mu_i + \rho_i + d + \delta_i {Q_i}^n - \beta {S_i}^n)\left(\frac{\partial I}{\partial t} + ...\right),\\
\Phi_{I_Q} &= -\frac{C_4h^2}{12}\left(\frac{\partial^4 I_Q}{\partial x^4}\right) + \tau(d + \nu_i + \mu_q + \rho_q)\left(\frac{\partial I_Q}{\partial t} + ...\right),\\
\Phi_Q &= -\frac{C_5h^2}{12}\left(\frac{\partial^4 Q}{\partial x^4}\right) + \tau(\psi)\left(\frac{\partial Q}{\partial t} + ...\right)\\
\Phi_V &= -\frac{C_6h^2}{12}\left(\frac{\partial^4 V}{\partial x^4}\right) + (d + \beta_v)\left(\frac{\partial V}{\partial t} + ...\right),
\end{aligned} \tag{5.21}$$

which also go to zero as τ,h becomes zero. For this reason, the order of accuracy of this numerical method is $h^2 + \tau$.

5.3. **Results.** By solving the system (5.2)-(5.7) with the values of parameters that were extracted and discussed in sections 3 and 4, taking the values $C_i = 0.01$ and $i = 1, 2, 3, 4, 5, 6$.
The Neumann boundary condition states that in complete lockdown, nobody can leave or enter the region. We can see in Figure 7 that the numerical solution at the pandemic equilibrium state at the selected parameters has good agreement with the chosen parameters.
All classes attain their maximum value in a specific region x and then decrease when they go away from this area.

6. Effects of Parameters

The value of each parameter in the model affects the spread of the disease. The most important issue in controlling epidemics is creating lockdowns to reduce relationships between individuals. In these models (temporal and spatio-temporal), we studied the effect of some parameters on infection classes I and I_Q. These models, represents the rate of infectious contact, which in turn affects the increase or decrease in the number of infected people, as shown in Figure 8. The lower the value of β decrease the infection rate, which indicates that the lack of contact between people leads to the disappearance of the epidemic or at least a decrease in cases of disease. On the other hand, as shown in Figure 9, by reducing ν_i, which represents the transmission of people from I_Q to I class , the number of infections decreases with the passage of time, which shows the role of isolation in reducing the spread of the disease. We also note an increase in μ_q , which represents the percentage of people recovering from the disease and were under lockdown, significantly reducing the number of infected people and under lockdown, as shown in Figures 10(b) and 10(d), but the percentage of infected people continues to increase as in Figures 10(a) and 10(c). In Figure 11, we made a comparison of different values of δ_s and their impact on the spread of the epidemic, where δ_s represents the rate of imposing the lockdown on healthy people who are exposed to infection. We find that by increasing the percentage of isolation, the number of epidemic infections decreases significantly.

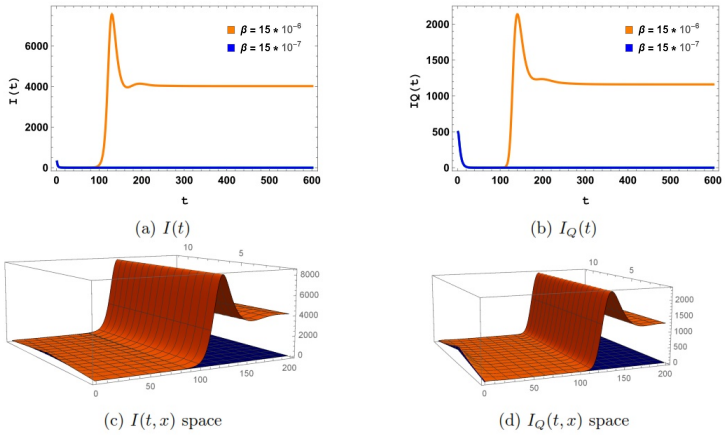

(a) $I(t)$ (b) $I_Q(t)$

(c) $I(t,x)$ space (d) $I_Q(t,x)$ space

FIGURE 8. Numerical simulation of I and I_Q with different values of $\beta = 15 * 10^{-6}$ and $15 * 10^{-7}$.

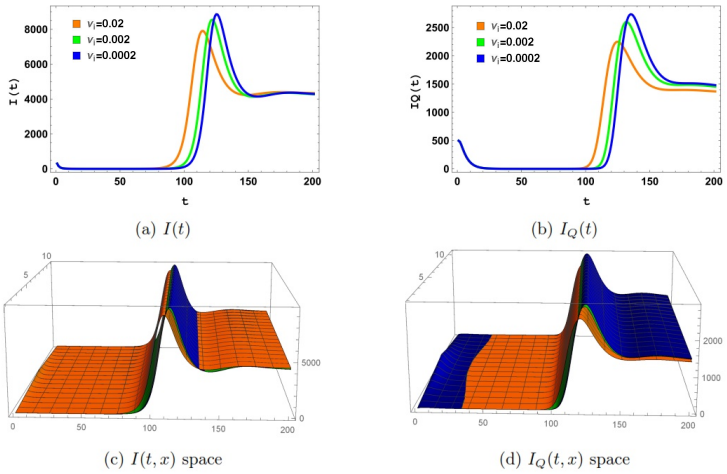

(a) $I(t)$ (b) $I_Q(t)$

(c) $I(t,x)$ space (d) $I_Q(t,x)$ space

FIGURE 9. Numerical simulation of I and I_Q with different values of $\nu_i = 0.02, 0.002, 0.0002$.

7. Conclusion

In this paper, a comprehensive numerical study of lockdown-vaccination models for COVID-19 is presented, focusing on both temporal and spatio-temporal aspects. The reproduction number is discussed as a crucial indicator for estimating the spread of the virus. The analysis includes a sensitivity analysis to assess the pandemic parameters. Moreover, the stability regions of the temporal model have been investigated. The numerical scheme applied to the spatio-temporal model is stable and has accuracy of order $(h^2+\tau)$. Numerical schemes such as CFD and RK-5 methods are employed to analyze the numerical results and facilitate comparison under various parameters. The findings have provided valuable insights into the control and mitigation of COVID-19, contributing to our understanding of the disease dynamics and the effectiveness of different intervention strategies. The graphical results of spatio temporal model showed that all classes attain their maximum value in a specific region and then decrease when people go away from this area, which means that lockdown is an excellent control for decreasing infection. We discussed the effect of some parameters on controlling the spread of infection between individuals. Results showed that β and ν_i have a direct impact on the number of infections $I(t)$, so that $I(t)$increase or decrease by increasing or decreasing them,

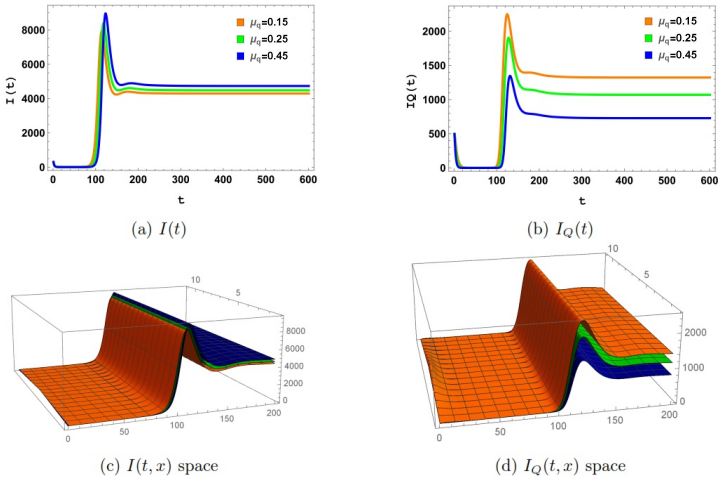

(a) $I(t)$ (b) $I_Q(t)$

(c) $I(t,x)$ space (d) $I_Q(t,x)$ space

FIGURE 10. Numerical simulation of I and I_Q with different values of $\mu_q = 0.15, 0.25, 0.45$.

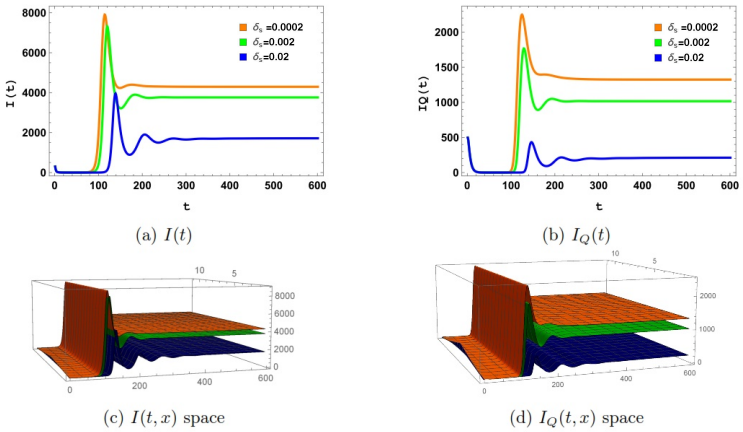

(a) $I(t)$ (b) $I_Q(t)$

(c) $I(t,x)$ space (d) $I_Q(t,x)$ space

FIGURE 11. Numerical simulation of I and I_Q with different values of $\delta_s = 0.02, 0.002, 0.0002$.

while μ_q have an inverse impact on $I(t)$ and a direct impact on $I_Q(t)$ and finally δ_s which have an inverse impact on both $I(t)$ and $I_Q(t)$, so an increase in δ_s leads to a decrease in $I(t)$ and $I_Q(t)$. This showed the importance of applying lockdown to reduce infection and control it. Overall, this study contributes to the existing knowledge base by providing a mathematical framework and numerical analysis of COVID-19 lockdown-vaccination models. The findings give critical insights for policymakers and healthcare professionals, allowing them to implement effective methods to limit viral transmission and mitigate its effects on public health and the economy. The ongoing study and fine-tuning of these models promise to increase our understanding of the intricate dynamics of infectious diseases, improving evidence-based decision-making in the context of pandemics.

AVAILABILITY OF DATA AND MATERIALS

Data sharing does not apply to this article because no datasets were created or analyzed during the current investigation.

Competing interests

The authors have declared that they have no competing interests.

Authors' contributions

The authors declare that the work was carried out in partnership with equal responsibility. All authors reviewed and approved the final manuscript.

Acknowledgment

All authors thank the journal's editor-in-chief, the editor who follows up on the work, and all journal employees.

Funding

No Funding.

References

[1] A. R. Adem, T. S. Moretlo, and B. Muatjetjeja, *A generalized dispersive water waves system: Conservation laws; symmetry reduction; travelling wave solutions; symbolic computation*, Partial Differ Eqn Appl Math., *7*(100465) (2022).

[2] P. Agarwal, M. A. Ramadan, A. A. M. Rageh, and A. R. Hadhoud, *A fractional-order mathematical model for analyzing the pandemic trend of COVID-19*, Math Meth Appl Sci., *45*(8) (2022), 4625–4642.

[3] K. K. Ali, S. B. G. Karakoc, and H. Rezazadeh, *Optical soliton solutions of the fractional perturbed nonlinear schrodinger equation*, TWMS Journal of Applied and Engineering Mathematics, *10*(4) (2020), 930–939.

[4] K. K. Ali, S. M. Mona, M. I. Abdelrahman, and M. A. Shaalan, *Analytical and Numerical solutions for fourth order Lane-Emden-Fowler equation*, Partial Differ Eqn Appl Math., *6*(100430) (2022).

[5] O. A. Arqub and B. Maayah, *Adaptive the Dirichlet model of mobile/immobile advection/dispersion in a time-fractional sense with the reproducing kernel computational approach: Formulations and approximations*, International Journal of Modern Physics B,*37*(18) (2023), 2350179.

[6] S. A. Baba, A. Yusuf, K. S. Nisar, A. Abdel-Aty, and T. A. Nofal, *Mathematical model to assess the imposition of lockdown during COVID-19 pandemic*, Result in Phys., *20*(103716) (2021), 1–7.

[7] M. Banan and A. Omar, *Hilbert approximate solutions and fractional geometric behaviors of a dynamical fractional model of social media addiction affirmed by the fractional Caputo differential operator*, Chaos, Solitons & Fractals, *10*(100092) (2023).

[8] M. Banan, A. Omar, A. Salam, and A. Hamed, *Numerical solutions and geometric attractors of a fractional model of the cancer-immune based on the Atangana-Baleanu-Caputo derivative and the reproducing kernel scheme*, Chinese Journal of Physics, *80* (2022), 463–483.

[9] S. K. Biswas, J. K. Ghosh, S. Sarkar, and U. Ghosh, *COVID-19 pandemic in India: a mathematical model study*, Non. Dyn., *102*(1) (2020), 537–553.

[10] Y. Chayu and W. Jin, *A mathematical model for the novel coronavirus epidemic in Wuhan*, China Math biosc and eng., *17*(3) (2020), 2708–2724.

[11] S. Djaouea, G. G. Kolayea, H. Abboubakar, A. A. Ari, and I. Damakoa, *Mathematical modeling analysis and numerical simulation of the COVID-19 transmission with mitigation of control strategies used in Cameroon*, Chaos, Solit & Fract., *139*(110281) (2020), 1–15.

[12] A. Fatemeh, S. Manmohan, and R. David, *Modelling of tumor cells regression in response to chemotherapeutic treatment*, Appl Math Mode., *48*(5) (2017), 96–112.

[13] S. B. G. Karakoc, K. K. Ali, and D. Y. Sucu, *A new perspective for analytical and numerical soliton solutions of the Kaup−Kupershmidt and Ito equations*, Journal of Computational and Applied Mathematics, *421*(114850) (2023).

[14] A. F. Koura , K. R. Raslan, K. K. Ali, and M. A. Shaalan, *Numerical analysis of a spatio-temporal bi modal coronavirus disease pandemic*, Appl Math and Inf Sci., *16*(5) (2022), 729–737.

[15] A. J. Kucharski, T. W. Russell, C. Diamond, Y. Liu, and J. Edmunds, *Early dynamics of transmission and control of COVID-19: a mathematical modelling study*, Inf Dise., *20*(5) (2020), 553–558.
[16] B. Maayah, A. Moussaoui, S. Bushnaq, and O. A. Arqub, *The multistep Laplace optimized decomposition method for solving fractional-order coronavirus disease model (COVID-19) via the Caputo fractional approach*, Demonstratio Mathematica, *55*(1) (2022), 963–977.
[17] M. Mandal, S. Jana, S. K. Nandi, A. Khatua, S. Adak, and T. K. Kar, *A model based study on the dynamics of COVID-19, prediction and control*, Chaos, Solit & Fract., *136*(109889) (2020), 1–12.
[18] H. Mohammadi, S. Kumar, S. Rezapour, and S. Etemad, *A theoretical study of the Caputo-Fabrizio fractional modeling for hearing loss due to Mumps virus with optimal control*, J of Chaos, Solit & Fract., *144*(110668) (2021).
[19] R. P. Mondaini and P. M. Pardalos, *Mathematical modelling of biosystems*, Sprin Sci & Bus Media, 2008.
[20] C. Rothe, M. Schunk, P. Sothmann, G. Bretzel, G. Froeschl, C. Wallrauch, and et al., *Transmission of 2019-nCoV infection from an asymptomatic contact in Germany*, N Eng J of Med., *382*(10) (2020), 970–971.
[21] N. H. Tuan, H. Mohammadi, and S. Rezapour, *A mathematical model for COVID-19 transmission by using the Caputo fractional derivative*, J. of Chaos, Solit. and Fract., *140*(110107) (2020).
[22] J. A. M. Valle, *Predicting the number of total COVID-19 cases and deaths in Brazil by the Gompertz model*, Non. Dyn., *102*(4) (2020), 2951–2957.
[23] D. Wrapp, N. Wang, K. S. Corbett, J. A. Goldsmith, C. Hsieh, O. Abiona, and et al., *Cryo-EM structure of the 2019-nCoV spike in the prefusion conformation*, Science., *367*(6483) (2020), 1260–1263.
[24] Z. Zhang, A. Zeb, O. F. Egbelowo, and V. S. Erturk, *Dynamics of a fractional order mathematical model for COVID-19 epidemic*, Adv Differ Equ., *420* (2020), 1–16.